Journal of The Electrochemical Society, **153** (6) H111-H114 (2006)
0013-4651/2006/153(6)/H111/4/$20.00 © The Electrochemical Society

Improvement of Field-Emission Properties of Screen Printed Carbon Nanotube Films via Argon Plasma Treatment

Jung-Ah Lee,[a,b] Jin-Woo Lee,[a] Dae-Sung Yoon,[a] Kyeong-Kap Paek,[c] Yun-Hi Lee,[b] and Byeong-Kwon Ju[d,z]

[a]*Microsystem Research Center, Korea Institute of Science and Technology, Seongbuk-gu, Seoul 136-791, Korea*
[b]*Department of Physics, and* [d]*Department of Electrical Engineering, Korea University, Seongbuk-gu, Seoul 136-701, Korea*
[c]*Department of Electronic Engineering, Daejin University, Pocheon, Gyeonggi-do 487-711, Korea*

In this paper, we describe an effective surface treatment to improve the field emission site density. The carbon nanotube (CNT) films fabricated by a screen printing process have been exposed to Ar plasma for varying durations and their field emission characteristics have been measured. The CNT films, after applying an Ar plasma treatment, have excellent field emission characteristics with very high emission current and low threshold fields. Scanning electron microscopy showed the contamination removal from the surface of the CNT films, and transmission electron microscopy showed the structural modification of the CNT walls after exposure to Ar plasma. Raman results showed that the particles generated by the deformation of the CNT structure had characteristics of both single-wall carbon nanotubes (SWCNTs) and multiwall carbon nanotubes (MWCNTs). We attribute improvement of field emission properties to the changes of the geometrical structure of the local emission region in MWCNTs.
 [DOI: 10.1149/1.2186770]

Manuscript submitted September 23, 2005; revised manuscript received January 27, 2006. Available electronically April 10, 2006.

Electron field emission from CNTs (carbon nanotube)[1,2] for electron emission sources has been investigated for many years because of its role in the development of efficient flat panel displays[3-5] and back lights of liquid crystal displays, and in other fields.[6-10] Reports have stated that field emission is dependent on the direct parameters of CNTs such as the number of walls,[11,12] the shape and structure of the tips,[13] and indirect parameters such as surface treatment and CNT-alignment methods[14] on a substrate. Recent works on CNT field emission are focused on several post-treatment methods and new growth method of CNTs to improve the uniformity and density of the electron emission site. Plasma surface treatment has been used as one of the post-treatment methods to improve the field emission properties of carbon-based materials.[15-18] For example, hydrogen, oxygen, and argon plasma are all found to improve the field emission properties of carbon-based material films by changing the atomic configurations on the surface.[8,19,20]

However, in spite of the experimental progress, low emission site density (ESD) and nonuniform emission remain the key issues to be addressed for displays. In addition, the properties of surface-treatment induced defects in multiwall carbon nanotubes (MWCNTs) are not yet well understood.[7] In this paper, we discuss the change of morphology, microstructures, and field emission properties of CNT films treated by argon plasma.[21-23]

As a result, we have found not only that argon plasma treated CNT films had the enhanced field emission properties, but also that surface-treatment induced defects of CNT films showed the possibility as linear electron emission sources.

Experimental

The CNT paste was made of a multiwall CNT (ILJIN Nanotech Co., Ltd., Korea), a glass frit, a glass frit solvent (SEM-COM Co.), a dispersing agent, and an organic binder. The organic binder includes ethyl cellulose (Sigma Chemical Co.) and organic solvent (SK Corp., Korea). Table I shows the ingredient of CNT paste. Figure 1 shows the process to fabricate CNT paste and CNT-FED (field emission display). To prepare the organic binder, ethyl cellulose was mixed with organic solvent by stirring. The multiwall CNT (MWCNT) used in this study was dispersed by the ultrasonication treatment in ethanol. About 0.6 g of MWCNT was added into 40 mL of 99.9% ethanol. The mixture was stirred for 30 min. After stirring, the mixture was placed in an ultrasonic bath and sonicated at 40°C for 20 min. The MWCNT was then separated from the fine filter paper (Advantec, Tokyo, Japan) and was prepared by evaporation of ethanol. The prepared MWCNT powder was mixed with glass frit, glass frit solvent, and organic binder materials to make a printable paste. Those materials were mixed together well by using a porcelain mortar for 1 h.

The CNT cathode plate was prepared by the screen printing method. The CNT paste for CNT-film emitters was printed on indium-tin oxide (ITO) coated soda-lime glass substrate. The cathode electrodes were prepared with no patterning. CNT paste-coated ITO glass substrate was heat treated under nitrogen gas flow to remove the contamination and to obtain good adhesion of CNT paste on an ITO substrate. The sintering temperature increased at a rate of 5°C/min. After the temperature reached 350°C, the heat treatment lasted for 10 min at 350°C.

We used Ar plasma treatment to study the correlation between surface treatment and field emission properties. Ar plasma surface treatment was performed by using reactive ion etching (RIE). RIE conditions were as follows: a power of 200 W, a pressure of 39.997 Pa, an argon flow of 30 sccm at treatment times of 2, 5, 8, and 10 min. After surface treatments, the morphology of CNTs were analyzed by field emission scanning electron microscopy (FESEM: S-4300, Hitachi, Tokyo, Japan). High-resolution transmission electron microscopy (HRTEM: JEM-3000F, JEOL, Tokyo, Japan) was used to characterize the microstructure of the nanotubes. The structural changes in the CNT films according to surface treatments were investigated by using a Raman spectrometer (Triple Raman Spectrometer: Jobin Yvon T64000) at 514.5 nm (Ar laser) in 100 mW.

The field emission property was measured in a vacuum field emission system that provided power between an MWCNT plate printed on the ITO glass as a cathode and a phosphor paste printed on the ITO glass as an anode. The base pressure of the field emission chamber was $\sim 1.333 \times 10^{-4}$ Pa. The measurements were made by applying voltages up to 2600 V across the anode and the cathode. The field emission of the CNT films was characterized in the con-

Table I. Chemical composition of the CNT paste.

Paste	Component portion (%)
MWCNT	4.62
Ethyl cellulose solution	30.77
Glass-frit	10.77
Glass-frit solvent	46.15
Dispersing agent	7.69

[z] E-mail: bkju@korea.ac.kr

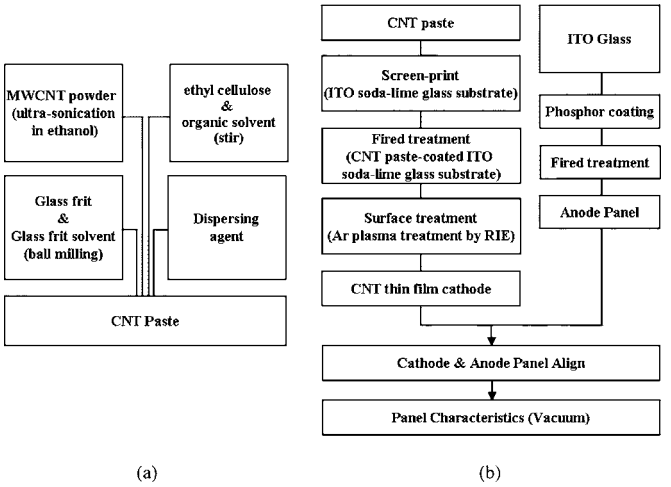

Figure 1. Fabrication process flow of (a) CNT paste and (b) CNT-FED.

ventional diode structure (3 in. 900 μm anode-cathode gap). In addition, the field emission images were taken by using a digital camera to compare the field emission characteristics before and after surface treatment.

Results and Discussion

The correlation between surface treatments and field emission properties of the screen printed CNT films was investigated. FESEM, HRTEM, and Raman spectroscopy showed the changes in the prepared samples. Figure 2 shows the FESEM images of the screen printed CNT films before and after Ar plasma surface treatment. Figure 2a shows the surface state of mixing both constituents of CNT paste and CNTs. From the image, it is very obvious that there are many coating impurities on the surface of nanotubes, such as the sintered glass-frit and amorphous carbon particles. Figure 2b presents an FESEM image of the CNT films after surface treatment, which illustrates the clean surface of the CNT films and a number of CNT deformations due to Ar ion bombardment. Figure 2c shows a cross-sectional FESEM image of CNT films. The consolidation of the CNT paste material and its bonding to the ITO substrate are accomplished through a thermal treatment.

To examine any changes in the surface and/or structural properties after the treatment, we performed HRTEM. Figure 3 shows HRTEM images of the structural variation in the CNTs occurring before and after Ar plasma treatment. Figure 3a shows an HRTEM image of MWCNTs used in this experiment. Figure 3b and c are HRTEM images of the CNT structure after the ion impinging. Figure 3b shows an HRTEM image of the transformed structure on MWCNTs by Ar plasma treatment. After plasma treatment, the surface topography of CNTs changed and many curve segments outgrew densely along the nanotube walls as shown in Fig. 3b. This change may be due to the defect generated on CNT walls having partly weak structure. Figure 3c is an HRTEM image of CNT tip after surface treatment. According to the theory of CNT field emission, electrons transport along the tube and can be emitted only from the CNT tip. However, the CNT tip in Fig. 3c is spherical. These transforms of CNTs may serve as an increase of electron emission site density to emit more than electrons; then, field emission properties could be enhanced.

In this paper, we used Raman spectroscopy to characterize the lattice damage of ion-irradiated solids. Raman characterization is a relatively easy and unique tool that can be used to characterize the structure of CNTs without destroying the sample.[24-26] Raman spectra covering the frequency range of 100–2000 cm^{-1} on five kinds of screen printed CNT films were recorded, and the results are shown in Fig. 4a and b. We looked into the total trend of Raman spectrum before and after surface treatment.

Figure 4a shows the result of Raman scattering measured in the frequency range of 100–700 cm^{-1}. The spectrum obtained in this region shows seven components. The peak was measured at 147 cm^{-1} corresponding to one of the peaks of the radial breathing modes (RBM) of SWCNTs,[24,25] and the peak at $\sim$500 cm^{-1} could be seen in the Raman spectrum of SWCNTs.[27] Our results were contrary to the fact that the RBM, in the case of MWCNTs, disappears owing to decoupling of the RBM.[26] The peaks at $\sim$212 and $\sim$287 cm^{-1} could be seen in the Raman spectrum of MWCNTs.[26,28] A peak at 287 cm^{-1} could be attributed to the radial nanotube breathing mode.[29] The origin of the peak at 287 cm^{-1} cannot be clearly identified, but it is estimated to be based on a very small diameter nanotube.[28] The peak at $\sim$440 cm^{-1} is close to two calculated E_{1g} and E_{2g} modes of armchair SWNTs.[27,30] It could therefore be interpreted as a vibration of large diameter MWNTs present in our samples. The reason the other peaks appeared in Fig. 4a is unclear, but it is likely that primarily the presence of CNT paste composition in Fig. 2c or the transformed structure of MWCNTs contributes to the Raman signals.

Figure 4b shows the result of Raman spectroscopy measured in the frequency range of 1200–1800 cm^{-1}. Generally, there are important peaks, so-called D- and G peaks, in Raman analysis of carbon-based materials. The D band gives information on the crystalline quality of the samples. The peaks near 1340–1355 cm^{-1} in Fig. 4b are due to the D peak. The G band is characteristic of graphitic carbon structures. Raman peaks in the 1550–1575 cm^{-1} are known as the G peaks.

The strength of the D line relative to the G line is a measure of the amount of disorder in the nanotube material.[31] The relative intensity rates (I_D/I_G) of the CNT films with time variation of the surface treatment were 0.941, 0.921, 0.962, 0.947, and 0.940, respectively. From the relative intensity of both nontreated and 2 min surface-treated samples, it could be interpreted that the overall crystalline quality of the nontreated film is lower than that of the 2 min surface-treated sample.[28] From these results mentioned above, it may be possible to get improved field emission properties. The conclusion about crystalline properties from the other three relative intensities is currently unclear. The reason is that these three relative intensities may be based not only on a dedicated theoretical analysis but also on a very tentative result. While the position of the Raman peaks in both nontreated and surface-treated CNT films was similar, their line strengths and widths are not. The linewidths of the nontreated MWCNT films are considerably broader than those of the

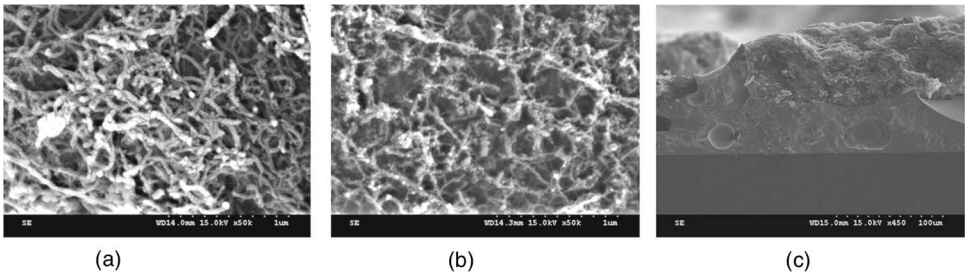

Figure 2. FESEM images of screen printed CNT films (a) before and (b) after Ar plasma treatment, and (c) a cross-sectional FESEM image of screen printed CNT films.

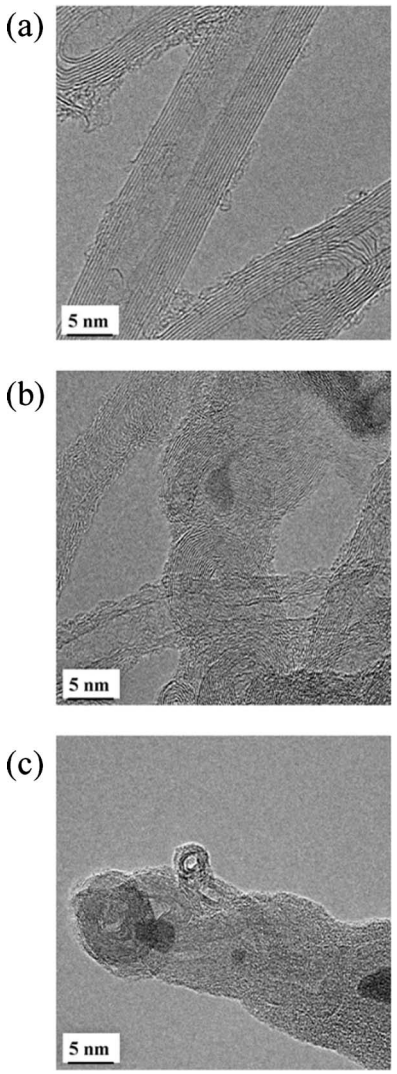

Figure 3. HRTEM images of screen printed CNT films (a) before; (b) and (c) after Ar plasma treatment.

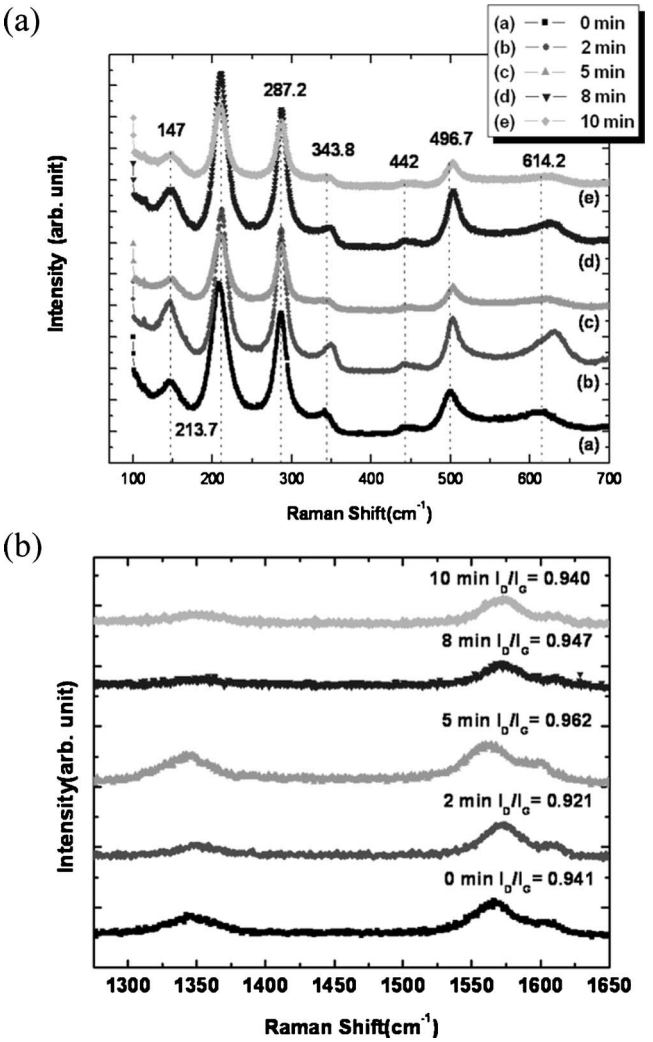

Figure 4. Raman spectra measured in the range of (a) 100–700 cm^{-1}; (b) 1200–1800 cm^{-1} of screen printed CNT films with different duration times of Ar plasma treatment.

surface-treated films. This is a consequence of the presence of impurities. The Raman signal sums up the contributions from the carbon nanotubes and the CNT paste composition. It is shown that the similarity of Raman peak positions appeared, because the skin depth of the laser light in disordered carbon materials is 80–100 nm.[32] With all of the contents mentioned above, Fig. 4 shows that the properties of surface-treated CNT films could be either SWCNTs or MWCNTs, which are considered to be related to the deformation effect of CNTs induced by surface treatments.

Figure 5 shows field emission images of the CNT films at a field of 2.9 V/μm. Figure 5a is a field emission image of untreated CNT films. There are a few very bright spots called hot spots, which cause poor emission uniformity. However, after post-treatment, the uniformity of emission from the CNT films improved as shown in Fig. 5b, because surface treatments effectively removed contaminants, such as organic materials and amorphous carbon, remaining on CNT-film emitters.

Figure 6 shows electron field emission properties of the CNT films before and after Ar plasma surface treatment. Figure 6a shows a plot of the emission current versus the applied voltage characteristics of the CNT films before and after surface treatment. The threshold voltage of the CNT films at an electrical field of 2.9 V/μm was the lowest in the 2 min surface-treated sample. According to the treatment time, the electron emission current of the CNT films at an electrical field of 2.9 V/μm ranged from 0.3 to 10.4 mA. Figure 6b shows the Fowler-Nordheim (FN) plots corresponding to Fig. 6a. The Fowler-Nordheim theory is the most commonly used model for field emission analysis. The total current I as a function of the local field at the emitter surface F is approximately given by

$$I \propto (F^2/\phi)\exp(B\phi^{3/2}/F)$$

with $B = 6.83 \times 10^9[VeV^{-3/2}m^{-1}]$, ϕ is work function, and β is field enhancement factor. F is usually taken as $F = \beta E = \beta V/d$, where V is the applied potential, d the distance between cathode and

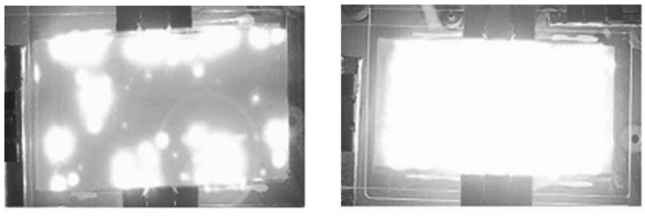

Figure 5. Field emission images of (a) before and (b) after Ar plasma treatment.

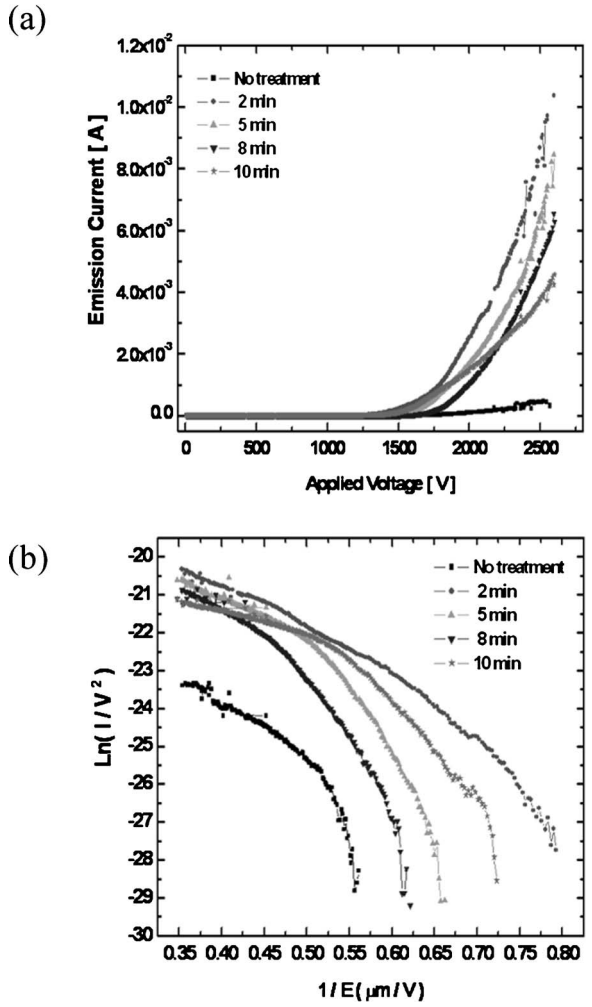

Figure 6. (a) *I-V* characteristics; (b) FN plots of screen printed CNT films before and after Ar plasma treatment.

anode, and $E = V/d$ the macroscopic field. In an FN plot, one should obtain a slope that depends on ϕ, β, and d.[11]

The field enhancement factor β is associated with geometrical shape of materials and inversely proportional to the slope of FN plots. In Fig. 6b, the slope of the FN plot at 2 min is the minimum value, which means that the field enhancement factor appears as the maximum value at 2 min. Accordingly, the field emission properties are enhanced. Though CNTs show excellent electron field emission characteristics at their tips, CNTs aligned on a substrate by a screen-printing process are random or disordered. Then, it is thought that parts other than CNT tips, i.e., bodylike walls transformed into spherical forms, play a major role as the emitter and improve electron emission characteristics.

Our experimental results have the same tendency, compared to the report of Ref. 33, where field emission arises from laterally aligned CNTs superior to that from vertically aligned CNTs. In addition, one report says that the plasma surface treatment using NH_3[10] gives occasion for changes in the structure of CNT walls, and enhances the electron field emission properties. Consequently, these reports were in agreement with our conclusions. We believe the Ar plasma surface treatment is an efficient method, which can produce excellent electrical characteristics to increase electron emission site density.

Conclusions

For improvement of field emission characteristics, the CNT film cathodes made by a screen printing process were exposed to Ar plasma. The field emission characteristics became better after surface treatment, and good electrical properties appeared for 2 min in one of the surface-treated films. To understand the effects of surface treatment, we characterized the surface morphology properties of CNT films and structural properties of CNTs by FESEM and HR-TEM. The surface state of the CNT films was cleaned after post-treatment. The deformation particles of CNTs had characteristics of both MWCNTs and SWCNTs by Raman analysis. In summary, the appearance of the deformation particles of CNTs results in an increase of the field emission properties. These results suggested that CNTs could be used as linear field emission sources.

Acknowledgment

This research has been supported by the Intelligent Microsystem Center (IMC), which carries out one of the 21st century's Frontier R&D Projects sponsored by the Korea Ministry of Commerce, Industry and Energy.

Korea University assisted in meeting the publication costs of this article.

References

1. S. Iijima, *Nature (London)*, **354**, 56 (1991).
2. S. Iijima and T. Ichihashi, *Nature (London)*, **363**, 603 (1993).
3. A. G. Rinzler, J. H. Hafner, P. Nikolaev, L. Lou, S. G. Kim, D. Tomanek, P. Nordlander, D. T. Colbert, and R. E. Smalley, *Science*, **269**, 1550 (1995).
4. W. A. de Heer, A. Châtelain, and D. Ugarte, *Science*, **270**, 1179 (1995).
5. P. G. Collins and A. Zettl, *Appl. Phys. Lett.*, **69**, 1969 (1996).
6. O. Zhou, H. Shimoda, B. Gao, S. Oh, L. Fleming, and G. Yue, *Acc. Chem. Res.*, **35**, 1045 (2002).
7. J. A. V. Pomoell, A. V. Krasheninnikov, K. Nordlund, and J. Keinonen, *J. Appl. Phys.*, **96**, 2864 (2004).
8. C. Y. Zhi, X. D. Bai, and E. G. Wang, *Appl. Phys. Lett.*, **81**, 1690 (2002).
9. K. S. Ahn, J. S. Kim, C. O. Kim, and J. P. Hong, *Carbon*, **41**, 2481 (2003).
10. J. Zhang, X. Wang, W. Yu, T. Feng, F. Zhang, Z. Zheng, Q. Li, and X. Liu, *Solid State Commun.*, **127**, 289 (2003).
11. J.-M. Bonard, J.-P. Salvetat, T. Stöckli, W. A. de Heer, L. Forró, and A. Châtelain, *Appl. Phys. Lett.*, **73**, 918 (1998).
12. Y. S. Shi, C.-C. Zhu, W. Qikun, and L. Xin, *Diamond Relat. Mater.*, **12**, 1449 (2003).
13. A. Buldum and J. P. Lu, *Mol. Simul.*, **30**, 199 (2004).
14. S. H. Jo, Y. Tu, Z. P. Huang, D. L. Carnahan, D. Z. Wang, and Z. F. Ren, *Appl. Phys. Lett.*, **82**, 3520 (2003).
15. C. Y. Li and A. Hatta, *Diamond Relat. Mater.*, **14**, 1780 (2005).
16. K. Yu, Z. Zhu, Y. Zhang, Q. Li, W. Wang, L. Luo, X. Yu, H. Ma, Z. Li, and T. Feng, *Appl. Surf. Sci.*, **225**, 380 (2004).
17. B. S. Satyanarayana, J. Robertson, and W. I. Milne, *J. Appl. Phys.*, **87**, 3126 (2000).
18. A. Ilie, A. Hart, A. J. Flewitt, J. Robertson, and W. I. Milne, *J. Appl. Phys.*, **88**, 6002 (2000).
19. A. Hart, B. S. Satyanarayana, W. I. Milne, and J. Robertson, *Appl. Phys. Lett.*, **74**, 1594 (1999).
20. D.-H. Kim, H.-S. Jang, C.-D. Kim, D.-S. Cho, H.-D. Kang, and H.-R. Lee, *Chem. Phys. Lett.*, **378**, 232 (2003).
21. ⟨http://www.iljinnanotech.co.kr/kr/material/r-6-2.htm⟩
22. M. Jinno, S. Bandow, and Y. Ando, *Chem. Phys. Lett.*, **398**, 256 (2004).
23. C. E. Hunt, O. J. Glembocki, Y. Wang, and S. M. Prokes, *Appl. Phys. Lett.*, **86**, 163112 (2005).
24. Y. Ando, X. Zhao, K. Hirahara, K. Suenaga, S. Bandow, and S. Iijima, *Chem. Phys. Lett.*, **323**, 580 (2000).
25. B. C. Liu, S. C. Lyu, T. J. Lee, S. K. Choi, S. J. Eum, C. W. Yang, C. Y. Park, and C. J. Lee, *Chem. Phys. Lett.*, **373**, 475 (2003).
26. X. Zhao, Y. Ando, L.-C. Qin, H. Kataura, Y. Maniwa, and R. Saito, *Chem. Phys. Lett.*, **361**, 169 (2002).
27. A. M. Rao, E. Richter, S. Bandow, B. Chase, P. C. Eklund, K. A. J. Williams, S. Fang, K. R. Subbaswamy, M. Menon, A. Thess, R. E. Smalley, G. Dresselhaus, and M. S. Dresselhaus, *Science*, **275**, 187 (1997).
28. M. Sveningsson, R.-E. Morjan, O. A. Nerushev, Y. Sato, J. Bäckström, E. E. B. Campbell, and F. Rohmund, *Appl. Phys. A*, **73**, 409 (2001).
29. M. S. Dresselhaus and P. C. Eklund, *Adv. Phys.*, **49**, 705 (2000).
30. P. C. Eklund, J. M. Holden, and R. A. Jishi, *Carbon*, **33**, 959 (1995).
31. M. S. Dresselhaus, M. A. Pimenta, P. C. Eklund, and G. Dresselhaus, in *Raman Scattering in Materials Science*, W. H. Weber and R. Merlin, Editors, p. 314, Springer, Berlin (2000).
32. B. S. Elman, M. Shayegan, M. S. Dresselhaus, H. Mazurek, and G. Dresselhaus, *Phys. Rev. B*, **25**, 4142 (1982).
33. Y. Chen, D. T. Shaw, and L. Guo, *Appl. Phys. Lett.*, **76**, 2469 (2000).